Nonlinear dynamics of a rotating flexible link

B. Sandeep Reddy [*], Ashitava Ghosal [†]

Abstract

This paper deals with the study of the nonlinear dynamics of a rotating flexible link modeled as a one dimensional beam, undergoing large deformation and with geometric non-linearities. The partial differential equation of motion is discretized using a finite element approach to yield four nonlinear, non-autonomous and coupled ordinary differential equations. The equations are non-dimensionalized using two characteristic velocities – the speed of sound in the material and a velocity associated with the transverse bending vibration of the beam. The method of multiple scales is used to perform a detailed study of the system. A set of four autonomous equations of the first order are derived considering primary resonances of the external excitation and one-to-one internal resonances between the natural frequencies of the equations. Numerical simulations show that for certain ranges of values of these characteristic velocities, the slow flow equations can exhibit chaotic motions. The numerical simulations and the results are related to a rotating wind turbine blade and the approach can be used for the study of the non-linear dynamics of a single link flexible manipulator.

Keywords: Flexible rotating beam, Nonlinear dynamics, Chaotic motion, Multiple scales analysis, Wind turbine blade

1 Introduction

Chaos is a critical phenomenon in nonlinear systems and has been extensively studied and observed in diverse fields such as physics, biological and chemical systems, communication channels and feedback control and is believed to occur in all complex nonlinear systems [1, 2, 3]. One of the first areas where chaotic motion was observed and studied extensively was in the nonlinear dynamics of one-degree-of-freedom mechanical oscillators [4, 5, 6, 7]. In the most well-known model of a nonlinear mechanical oscillator, the Duffing's equation [8], the spring stiffness is modeled with a cubic nonlinear term and for certain ranges of values of the damping coefficients and amplitude of the forcing, the system response is found to be chaotic. Chaotic motions have also been studied in multi-degree-of-freedom mechanical systems such as a double pendulum [9] and robot manipulators [10, 11, 12, 13, 14, 15]. In contrast to the Duffing's equation, the nonlinearity in the robot manipulator models is not in the stiffness term but in the configuration dependent inertia term or in the terms representing the feedback control. In such multi-degree-of-freedom systems, the model has more than two first-order ordinary differential equations (ODEs) which results in more difficult analysis and simulations. Xiao et al. [16] observed bifurcation and chaos in the transverse vibrations of an axial accelerating beam with geometric nonlinearities. Yu et al. [17] studied the bifurcation of a double pendulum at various critical points analytically to get explicit expressions for the bifurcation lines, and then numerically simulated the system to get period doubling bifurcation cascades leading to chaos.

In contrast to the extensive analysis of systems described with two or three first-order ODEs, very little work is available on analysis and study of nonlinear systems modeled with four or more ODEs. Some of the well-known studies involving four ODEs are Nayfeh et al. [18] where the motions near the hopf bifurcations of a non-conservative four dimensional autonomous system were studied. Using the method of multiple scales [19], the Hopf bifurcation problem was reduced to two differential equations for the amplitude and phase of the bifurcating cyclic solutions, and the stability of constant solutions to those equations determined the nature of bifurcation. In the work by Kumawat et al. [20], a parametric study of reduced order model of boiling water reactors, modeled by four first order differential equations, has been performed by using the multiple scales method, and the authors report sub-critical bifurcations at a particular value of fuel temperature. However, with an decrease in the fuel temperature coefficient of reactivity the bifurcation turns to

[*]Graduate Student, Department of Mechanical Engineering, Indian Institute of Science, Bangalore, India. Email: bsandeep@mecheng.iisc.ernet.in

[†]Corresponding Author, Professor, Department of Mechanical Engineering, Indian Institute of Science, Bangalore, India. Email: asitava@mecheng.iisc.ernet.in

supercritical implying global stability of the steady state operation in the linear stability regime. In this work, we investigate a set of four nonlinear ODEs arising from a simple model of rotating flexible beam undergoing large deformation.

In an earlier work, flexible link manipulators undergoing large deformations were modeled as beams with a nonlinear strain-displacement relation and the governing partial differential equation were discretized using a finite element technique to yield a set of four first-order, nonlinear ordinary differential equations [21]. The four first-order ODEs were written in a non-dimensionalised form using two characteristic velocities, namely the speed of sound and a velocity associated with the transverse bending vibrations of the beam. In this work, we analyse these four first order ODEs and show that for certain ranges of values of these characteristic velocities the system of equations representing the rotating beam can exhibit chaotic motions. We further show that these values of characteristic velocities are possible to obtain in a rotating blade of a wind turbine (modeled as a beam) or in a flexible link manipulator. This paper is organized as follows: In section 2, we briefly describe the rotating flexible beam and present the nonlinear ODEs used to model the undamped and damped rotating beam undergoing large deformation and present the non-dimensional form of the equations derived using the two characteristic velocities. In section 3, we present a multiple scales analysis of the system of four ODEs to derive the slow flow equations and analyze the system of equations for the undamped and damped case. In section 4, we examine the results obtained from numerical simulations to obtain better insight as to the range of characteristic velocities for which the system can exhibit chaos. In section 5, we present conclusions of this work.

2 Description of the rotating flexible beam

The modeling of a rotating flexible beam, undergoing large deformation and the derivation of equations of motion in a non-dimensional form is presented in reference [21]. These are presented in brief in this section.

The rotating link is schematically shown in figure 1 (a). The link is discretised into a finite number of beam elements, with all its nodal variables as described in figure 1 (b), defined in the body-fixed co-ordinate system $O_iX_iY_i$ with O_iX_i along the tangent at the $(2i-2)^{\text{th}}$ node of the system. The co-ordinate system OXY is the global

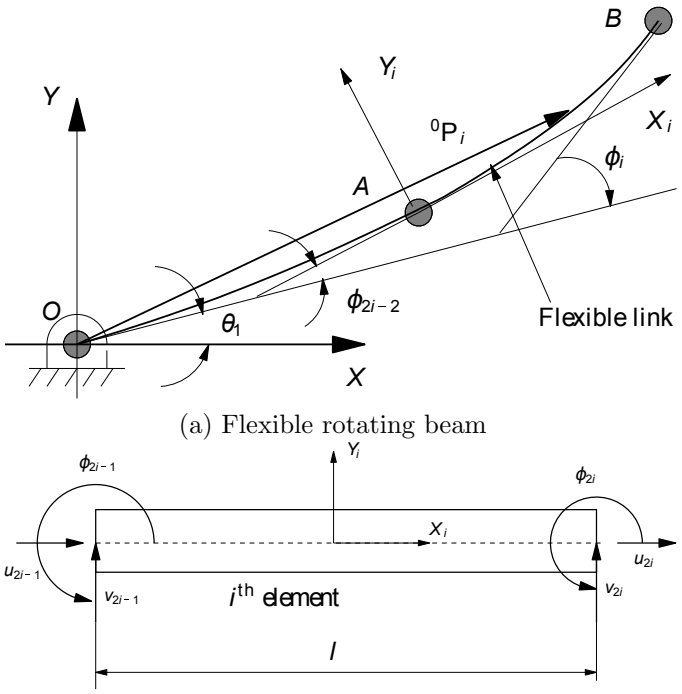

(a) Flexible rotating beam

(b) Planar beam element

Figure 1: Schematic of a rotating flexible beam and an i^{th} element

co-ordinate system as shown in figure 1 (a) and an arbitrary point on the flexible link, in the global coordinate system, is denoted by ${}^0\mathbf{P}_i$

The rotating flexible link is assumed to have constant cross-sectional area and uniform material properties and is assumed to undergo axial elongation in addition to transverse bending. From the figure 1, it can be observed that θ_1 is the global variable and $(u_{2i-1}, v_{2i-1}, \phi_{2i-1}, ..., u_{2i}, v_{2i}, \phi_{2i})$ are the nodal variables of the system. The index i refers to the ith discretized element (in Figure (1)a, OA is the first element, OB is the second element and so on) of the beam, whereas the total number of such elements of the beam is given by N. In our work, we consider only the first element, hence $N = 1$. The beam is assumed to undergo large deformations hence a nonlinear strain-displacement relationship needs to be used to describe the relation between the strain and the displacements. Following the development in reference [21], we can write

$$\epsilon_{xx} = \frac{\partial u_x}{\partial x} - y\frac{\partial^2 u_y}{\partial x^2} + \frac{1}{2}\left(\frac{\partial u_y}{\partial x}\right)^2 \tag{1}$$

where ϵ_{xx} denotes the normal strain, and u_y and u_x denote the longitudinal and transverse displacement at axis

$y = 0$ (see figure 1 (b)) respectively. The above strain-displacement equation can be used to obtain the strain energy of the system as

$$U = \frac{EA}{2}\int_0^l \left(\frac{\partial u_x}{\partial x}\right)^2 dx + \frac{EI}{2}\int_0^l \left(\frac{\partial^2 u_y}{\partial x^2}\right)^2 dx + \frac{EA}{2}\int_0^l \left(\frac{\partial u_x}{\partial x}\right)\left(\frac{\partial u_y}{\partial x}\right)^2 dx \quad (2)$$

where E, A, I, l denote the Young's modulus, cross-sectional area, moment of inertia of cross-section and length of the beam, respectively. It can be observed from equation (2), that the nonlinearity is quadratic and represents the geometric nonlinearity associated with transverse bending and axial deformation.

Following the developement in reference [21], the total kinetic energy of the beam can be obtained from the time derivative of the vector ${}^0\mathbf{P}_i$ and integration. It can be expressed as

$$T = \frac{1}{2}\dot{Q}^T[M]\dot{Q} \quad (3)$$

where $[M]$ is the mass matrix and Q is the vector of generalized coordinates given by $(\theta_1, S)^T$ with S denoting the vector of nodal variables given by $(u_1, v_1, \phi_1, ..., u_{2N}, v_{2N}, \phi_{2N})$ (see figure 1 (b)).

The total potential energy of the beam can be obtained from equation (2), and can be written as

$$V = \frac{1}{2}S^T([K] + [\Delta K(S)])S \quad (4)$$

where $[K]$ is the conventional stiffness matrix and $[\Delta K(S)]$ is the geometric stiffness matrix. From the potential and kinetic energy given by equations (3) and (4), the equations of motion can be derived using a Lagrangian formulation. The nonlinear differential equations can be schematically written as

$$[M(Q)]\{\ddot{Q}\} + ([K] + [\Delta K(Q_f)])\{Q_f\} + h(Q, \dot{Q}) = \{\tau\} \quad (5)$$

where $h(Q, \dot{Q})$ is the vector of Coriolis and centripetal terms, $\{\tau\} = [\Gamma, 0, 0, 0]^T$ is a vector of input torques and $Q_f = (0, u_2, v_2, \phi_2)^T$ is a vector of flexible variables. Equation (5) represents a set of four second-order ordinary differential equations.

The equations of motion (5) can be non-dimensionalized [21] using two characteristic velocities

$$U_g = \frac{1}{L}\sqrt{\frac{EI}{\rho A}}, \quad U_a = \sqrt{\frac{E}{\rho}}, \quad T = t/(L/U_g) \quad (6)$$

where U_a is the speed of sound and U_g is a characteristic speed associated with bending vibration [21] and T is a non-dimensional time. The quantity U_g is dependent on geometric and material properties of the beam whereas U_a is purely a material property. For a circular cross-section beam of radius R and length L, we can relate U_g and U_a as

$$U_g = \frac{1}{L}\cdot\sqrt{\frac{EI}{\rho A}} = \frac{1}{L}\cdot\sqrt{\frac{E}{\rho}}\cdot\sqrt{\frac{\pi R^4/2}{\pi R^2}} = \frac{U_a R}{L\sqrt{2}} \quad (7)$$

The above equation indicate that U_g *decreases* with larger L and smaller R, i.e., U_g is small for thinner and longer beams.

The equations of motion in the non-dimensional form can be written as

$$[\mathcal{M}(Q_f)]\ \{Q^{''}\} + \left(\mathcal{K} + \Delta\mathcal{K}(Q_f, \frac{U_a}{U_g})\right)\{Q\} + \mathcal{C}\{Q'\} + \{\mathcal{H}(Q, Q^{'})\} = \frac{\{\tau\}}{\rho A L U_g^2} \quad (8)$$

where $(\cdot)^{'}, (\cdot)^{''}$ represent the first and the second derivative with respect to non-dimensional time T, $\mathcal{M}$ is the 4×4 non-dimensional mass matrix, $\mathcal{K}$ and $\Delta\mathcal{K}$ are the 4×4 non-dimensional conventional and geometric stiffness matrices respectively, $\mathcal{H}$ is the 4×1 vector of non-dimensional centripetal and Coriolis terms, $\{\tau\} = [F\sin(\frac{\Omega L}{U_g}T), 0, 0, 0]^T$ with F and Ω denoting the amplitude and the frequency of forcing term (see Appendix 1 for details of the terms in equation (8)) and $\mathcal{C}\{Q'\}$ represents an added Rayleigh damping term of the form $\alpha[\mathcal{M}] + \beta[\mathcal{K}]$.

In this work we focus on U_g and show that for certain ranges of U_g, the system of four ODEs in equation (8) can exhibit chaos. For numerical simulations in section 4, we will use the values given in Table 1 and we assume the value of amplitude of forcing $F = \pi/2$ and the values of the Rayleigh damping coefficients as $\alpha = 0.02$ and $\beta = 0.02$. The reason for choosing the particular values of damping co-efficients α and β is that high damping increases stability and hence there is no chance of chaotic motion. Hence, we choose low values of α and β as given above to enable the possibility of exploring chaotic motion. It may be noted that the ρ and E values given in Table 1 are of E-glass which is used to make wind turbine blades and the value of L is for a 50 kW wind turbine made by Endurance Wind Power Ltd. [22]. The value of Ω is the operating angular speed of the wind turbine blade.

Table 1: Parameter values used in simulations

Parameter	Numerical Value
Material	E-Glass
ρ	2550 kg/m^3
E	80 (GPa)
U_a	$\sqrt{\frac{E}{\rho}} = 5601$ m/s
L	9 (m)
Ω	42 (rpm)

It maybe noted that the blade cross-section in not uniform in a wind turbine and the U_g value is not known. In section 4, we show that if the blade is assumed to have a uniform circular cross-section, then for certain values of U_g (and resulting value of the circular cross-section), the system of equations modeling the rotating blade can exhibit chaos.

3 Multiple scales analysis

The method of multiple scales examines the behavior of a nonlinear system of equations at various time scales to obtain insight into the behavior of a nonlinear dynamical system. Details of the method of multiple scales are available in Nayfeh [19] and examples of analysis of nonlinear systems using method of multiple scales can be found in references [23, 24, 25, 26] and in references contained in these works.

In this section, we apply the method of multiple scales to the set of equations given by (8) with and without the damping term. In this work, we order the nonlinearities, damping and excitation effects at the second order and study their effects at the slow time scale. We seek a uniform expansion for the solution of equations (8) in the form

$$x(t;\epsilon) = \epsilon x_{10}(T_0, T_1) + \epsilon^2 x_{11}(T_0, T_1) \tag{9}$$

where, ϵ is a small dimensionless measure of x which can be any of the variables (θ_1, U_2, V_2, ϕ_2), $T_0 = t$ is the fast scale associated with changes occurring at the forcing frequencies Ω and the natural frequencies ω_n, and $T_1 = \epsilon t$ is the slow scale associated with the modulations of the amplitudes and phases due to nonlinearities and resonances. Equation (9) ensures that the nonlinear effects in equations (8) appear at the second order. Ordering the damping and excitation effects so as to appear at the second order, we can rewrite the set of equations as:

$$[\mathcal{M}(Q_f)]\ \{Q^{''}\} + \left(\mathcal{K} + \Delta\mathcal{K}(Q_f, \frac{U_a}{U_g})\right)\{Q\} + \epsilon\left(\mathcal{C}\{Q^{'}\}\right) + \{\mathcal{H}(Q, Q^{'})\} = \epsilon\left(\frac{\{\tau\}}{\rho A L U_g^2}\right) \tag{10}$$

We perform a multiple scales analysis on equation (10) – the results for the undamped case can be obtained by setting the damping to zero. Substituting equations (9) into equation (10) and equating coefficients of like powers of ϵ, we obtain

Order ϵ

$$\begin{aligned}
&\frac{1}{3}D_0^2\theta_{10} + \frac{7}{20}D_0^2V_{20} - \frac{1}{20}D_0^2\phi_{20} = 0\\
&\frac{1}{3}D_0^2U_{20} + \frac{U_a^2}{U_g^2}U_{20} = 0\\
&\frac{7}{20}D_0^2\theta_{10} + 12V_{20} + \frac{13}{35}D_0^2V_{20} - 6\phi_{20} - \frac{11}{210}D_0^2\phi_{20} = 0\\
&-\frac{1}{20}D_0^2\theta_{10} - 6V_{20} - \frac{11}{210}D_0^2V_{20} + 4\phi_{20} + \frac{1}{105}D_0^2\phi_{20} = 0
\end{aligned} \tag{11}$$

where $D_n^2 = (\partial^2/\partial T_n^2)$. The solution of equations (11) is of the form

$$\begin{aligned}
\theta_{10} &= A_3e^{i\omega_3T_0} + A_4e^{i\omega_4T_0} + c.c.\\
U_{20} &= A_2e^{i\omega_2T_0} + c.c.\\
V_{20} &= C_{33}(A_3e^{i\omega_3T_0}) + C_{34}(A_4e^{i\omega_4T_0}) + c.c.\\
\phi_{20} &= C_{43}(A_3e^{i\omega_3T_0}) + C_{44}(A_4e^{i\omega_4T_0}) + c.c.
\end{aligned} \tag{12}$$

where $c.c$ stands for complex conjugate and the derivation of equation (12) is given in Appendix 2. The above equations are used for obtaining **Order** ϵ^2 equations next.

Order ϵ^2

$$\begin{aligned}
&\frac{1}{3}D_0^2\theta_{11} + \frac{7}{20}D_0^2V_{21} - \frac{1}{20}D_0^2\phi_{21} = -\frac{2}{3}D_0D_1\theta_{10}\\
&\alpha\left(-\frac{1}{3}D_0\theta_{10} - \frac{7}{20}D_0V_{20} + \frac{1}{20}D_0\phi_{20}\right) - \frac{2}{3}U_{20}D_0^2\theta_{10}\\
&\left(\frac{7}{20}V_{20} - \frac{\phi_{20}}{20}\right)D_0^2U_{20} - \frac{7}{10}D_0D_1V_{20} + \frac{1}{10}D_0D_1\phi_{20}\\
&+ U_{20}\left(\frac{D_0^2\phi_{20}}{20} - \frac{7D_0^2V_{20}}{20}\right) - \frac{2}{3}D_0U_{20}D_0\theta_{10}
\end{aligned}$$

$$\begin{aligned}
&\frac{1}{3}D_0^2U_{21} + \frac{U_a^2}{U_g^2}U_{21} = -\frac{\alpha}{3}D_0U_{20} - \frac{2}{3}D_0D_1U_{20}\\
&-\frac{U_a^2}{U_g^2}\left(\frac{3}{5}V_{20}^2 + \frac{\phi_{20}^2}{15} - \frac{V_{20}\phi_{20}}{10}\right) + \left(\frac{7V_{20}}{20} - \frac{\phi_{20}}{20}\right)D_0^2\theta_{10}\\
&+\left(\frac{7D_0V_{20}}{10} + \frac{D_0\theta_{10}}{3}\right)D_0\theta_{10}
\end{aligned} \tag{13}$$

$$\frac{7}{20}D_0^2\theta_{11} + 12V_{21} + \frac{13}{35}D_0^2V_{21} - 6\phi_{21} - \frac{11}{210}D_0^2\phi_{21} =$$
$$-\frac{7\alpha}{20}D_0\theta_{10} - \left(\frac{13\alpha}{35} + 12\beta\right)D_0V_{20} - \frac{26}{35}D_0D_1V_{20}$$
$$+\left(\frac{11\alpha}{210} + 6\beta\right)D_0\phi_{20} + \frac{11}{105}D_0D_1\phi_{20} - \frac{7}{10}D_0U_{20}D_0\theta_{10}$$
$$-\frac{7}{20}U_{20}D_0^2\theta_{10} - \frac{U_a^2}{U_g^2}\left(\frac{6}{5}V_{20} + \frac{\phi_{20}}{10}\right)U_{20} - \frac{7}{10}D_0D_1\theta$$

$$-\frac{1}{20}D_0^2\theta_{11} - 6V_{21} - \frac{11}{210}D_0^2V_{21} + 4\phi_{21} + \frac{1}{105}D_0^2\phi_{21} =$$
$$\frac{\alpha}{20}D_0\theta_{10} - \left(\frac{11\alpha}{210} + 6\beta\right)D_0V_{20} + \frac{11}{105}D_0D_1V_{20}$$
$$-\left(\frac{\alpha}{105} + 4\beta\right)D_0\phi_{20} - \frac{2}{105}D_0D_1\phi_{20} + \frac{1}{10}D_0U_{20}D_0\theta_{10}$$
$$-\frac{1}{20}U_{20}D_0^2\theta_{10} - \frac{U_a^2}{U_g^2}\left(-\frac{V_{20}}{10} + \frac{2\phi_{20}}{15}\right)U_{20} + \frac{1}{10}D_0D_1\theta_{10}$$

It is important to note that there are infinite number of eigenvalues and modes for a continuous systems. For nonlinear systems, the mode that is directly excited by an external excitation or indirectly excited by an internal resonance with one of the natural frequencies will survive and all other modes would decay in time. In this case, we consider an internal resonance between the second and third mode and a combination external resonance with third mode. In order to separate the secular terms, we introduce a detuning parameter as follows:

$$\omega_2 = 2\omega_3 + \epsilon\sigma_1, \quad \Omega = \omega_3 + \epsilon\sigma_2 \tag{14}$$

To determine the solvability conditions, we seek a particular solution free of secular terms corresponding to the terms proportional to $e^{i\omega_n T_0}$, in the form

$$\theta_{11} = \sum_{i=1}^{4} P_i(T_1)e^{i\omega_i T_0}, \quad U_{21} = \sum_{i=1}^{4} Q_i(T_1)e^{i\omega_i T_0} \tag{15}$$
$$V_{21} = \sum_{i=1}^{4} R_i(T_1)e^{i\omega_i T_0}, \quad \phi_{21} = \sum_{i=1}^{4} S_i(T_1)e^{i\omega_i T_0}$$

Substituting equation (15) on the left hand side of equation (13) and equations (12), (14) on the right hand side of equation (13), and equating the coefficients of the powers of $e^{i\omega_2 T_0}$ and $e^{i\omega_3 T_0}$, we can determine the solvability conditions, thus eliminating the secular terms (see [19] for details about this procedure). After applying the procedure we determine the solvability conditions as:

At $e^{i\omega_2 T_0}$

$$-\frac{2}{3}A_2^{'}(i\omega_2) + J_{22}A_3^2e^{-i\sigma_1 T_1} - A_2(i\omega_2)\frac{\alpha}{3} = 0 \tag{16}$$
$$\implies iA_2^{'} = \frac{3J_{22}}{2\omega_2}A_3^2e^{-i\sigma_1 T_1} \implies iA_2^{'} = J_2A_3^2e^{-i\sigma_1 T_1}$$

At $e^{i\omega_3 T_0}$

$$A_3^{'}(i\omega_3)\{Z_{11}Z_{w1} + Z_{31}Z_{w3} + Z_{41}Z_{w4}\}$$
$$+ A_2\overline{A}_3e^{i\sigma_1 T_1}\{Z_{12}Z_{w1} + Z_{32}Z_{w3} + Z_{42}Z_{w4}\}$$
$$+ A_3(i\omega_3)(Z_{d1}Z_{w1} + Z_{d3}Z_{w3} + Z_{d4}Z_{w4})$$
$$- \frac{Fi}{2}e^{i\sigma_2 T_1}Z_{w1} = 0$$
$$\implies A_3^{'} = -A_3J_{3d} + J_{31}e^{i\sigma_2 T_1} + J_{32}iA_2\overline{A}_3e^{i\sigma_1 T_1} \tag{17}$$

where $J_2 = (3J_{22}/2\omega_2)$, $J_{31} = (FZ_{w1}/2\omega_3L_1)$, $J_{32} = (L_2/\omega_3L_1)$, $J_{3d} = (L_{3d}/L_1)$ and the values of $J_{22}, Z_{11}, Z_{31}, ...$ are given in Appendix 2. Introducing the polar notation $A_n = a_ne^{ib_n}$ and using in equations (16-17), we get

$$a_2^{'} = -\frac{\alpha}{2}a_2 - J_2a_3^2\sin\gamma, \quad b_2^{'} = -J_2\frac{a_3^2}{a_2}\cos\gamma$$
$$a_3^{'} = -J_{3d}a_3 + J_{31}\cos\delta - J_{32}a_2a_3\sin\gamma \tag{18}$$
$$b_3^{'} = \frac{1}{a_3}J_{31}\sin\delta + J_{32}a_2\cos\gamma$$

where $\delta = \sigma_2T_1 - b_3$ and $\gamma = \sigma_1T_1 + b_2 - 2b_3$. Modifying coordinates using $x = a_2\cos\gamma$, $y = a_2\sin\gamma$, $z = a_3\cos\delta$ and $w = a_3\sin\delta$, we have the final set of four slow flow equations given by

$$\dot{x} = -\frac{\alpha x}{2} - \sigma_1 y + 2J_{32}xy + 2J_{31}\frac{yw}{z^2+w^2}$$
$$\dot{y} = -\frac{\alpha y}{2} + \sigma_1 x - J_2(z^2+w^2) - 2J_{32}x^2 - 2J_{31}\frac{xw}{z^2+w^2}$$
$$\dot{z} = -J_{3d}z - \sigma_2 w + J_{31} + J_{32}(xw - yz) \tag{19}$$
$$\dot{w} = -J_{3d}w + \sigma_2 z - J_{32}(yw + xz)$$

The above equations represent the damped slow flow equations of the system. For the undamped slow flow equations, we set $\alpha = 0$ and $\beta = 0$ in the above equations, and, as a result, the terms α and J_{3d} will vanish.

Dissipativity

To check if the system given by equation (19) is dissipative or not, we calculate the gradient of the volume enclosed by the system

$$\nabla V = \frac{\partial f_1}{\partial x} + \frac{\partial f_2}{\partial y} + \frac{\partial f_3}{\partial z} + \frac{\partial f_4}{\partial w} \tag{20}$$

where f_1, f_2, f_3, f_4 respectively, denote the four equations in (19). Substituting equation (19) into equation(20), we have

$$\nabla V = 2J_{32}y - \alpha + 0 - J_{32}y - J_{32}y - 2J_{3d} = -(\alpha + 2J_{3d}) \tag{21}$$

From equation (21), we can observe that the gradient is nonzero iff $\alpha+2J_{3d} > 0$, i.e., the system is dissipative and the volume enclosed by the system is not preserved for all values of parameter U_g. Hence, the system of equations can have chaotic attractors or repellors. For an undamped system, α and J_{3d} are zero, and hence the gradient for an undamped system, as given by equation (21), can be seen to be zero. This implies that the undamped system is conservative and the volume enclosed by such a system is preserved for all U_g. Such a system cannot have chaotic attractors and repellors.

The fixed points of the slow flow equations given by equations (19) are obtained by setting $\dot{x} = \dot{y} = \dot{z} = \dot{w} = 0$. We first consider the undamped slow flow equations obtained by setting α and J_{3d} as zero in equation (19). After simplification, the fixed point of the system are obtained as $(xe_1, 0, 0, we_1)$ where (xe_1, we_1) are given by

$$\begin{aligned} xe_1 &= \frac{N^{1/3}}{6J_{32}(\sigma_1 - 2\sigma_2)} + \frac{2\sigma_2^2(\sigma_1 - 2\sigma_2)}{3J_{32}N^{1/3}} + \frac{2\sigma_2}{3J_{32}} \\ we_1 &= \frac{J_{31}}{\sigma_2 - J_{32}xe_1} \end{aligned} \tag{22}$$

where

$$\begin{aligned} N = (\sigma_1 - 2\sigma_2)^2 \times & \\ \{8\sigma_2^3\sigma_1 + 16\sigma_2^4 + 108J_{32}J_{22}J_{31}^2 & \\ + 12J_{31}J_{32}\sqrt{\frac{3J_{22}(-4\sigma_2^3\sigma_1 + 8\sigma_2^4 + 27J_{32}J_{22}J_{31}^2)}{J_{32}}}\} & \end{aligned} \tag{23}$$

The fixed points of the undamped slow flow equations for different values of U_g can be computed from equation (22) and (23). The fixed points for representative U_g values are given in Table 2 below.

The damped slow flow equations given by equations (19) have *no fixed points* although the damped slow flow equations show the existence of an attractor. Since there are no fixed points, the attractor can be an attracting limit cycle.

Table 2: Fixed points of undamped slow flow equations

U_g	Fixed points
250	(-67.8988,0,0,-4.0000 +58.1750i), (-67.8988,0,0,-4.0000 -58.1750i), (0,0,0,2)
150	(0,0,0,0), (-24.3996,0,0,-0.5000 +77.6724i), (-24.3996,0,0,-0.5000 -77.6724i)
100	(0,0,0,0.1250), (-10.8228,0,0,-122.75-0.06199i), (-10.8228,0,0,123.5+0.06199i)
50	(0,0,0,0), (-2.6902,0,0,-27.5044 + 0.0004i), (-2.6902,0,0,27.5058 - 0.0004i)

4 Numerical simulation

The equations obtained in previous analysis have been simulated numerically to determine the existence of chaos for a given value of U_g. Some of the well-known ways to determine if a system is chaotic is by computing the Lyapunov exponent, Poincaré maps, phase portraits and bifurcation diagrams and auto-correlation functions [27]. In this work, we use Lyapunov exponents, phase portraits and Poincaré maps. Lyapunov exponents are a measure of the average rate of divergence of neighbouring trajectories of the system and a positive Lyapunov exponent for a given control parameter value would be sufficient condition for chaos. A Poincaré map is map formed by a cross sectional plane cutting the phase space orbits. While the flow of the orbit may be in continuous time, their intersection with the cross-sectional plane are in discrete time and the n-dimensional flow in continuous time is replaced by an $(n-1)$ dimensional iterated map. The Poincaré map, though by itself not a sufficient condition for chaos, gives an indication of possible mixing in the system. Phase portraits are studied to observe possible bifurcation in limit cycles with change in the control parameter. The calculation of Lyapunov exponents is demonstrated by Sandri [28]. The various other numerical algorithms for chaotic systems for computing Poincaré maps, phase portraits, etc. can be found in reference [27]. A method for computing bifurcation values is given by Tsumoto et al. [29].

To perform the numerical study of the system in equation (19), we use the parameters given in Table 1. All simulations were done using MATLAB 2012Rb [30] and *ode*15*s* solver was used to solve the differential equations. The relative and absolute tolerances were kept at 10^{-6} and 10^{-9} respectively. Figures 2 and 3 show the numerical simulation results of the undamped slow flow equations given by setting α and J_{3d} as zero in equation (19).

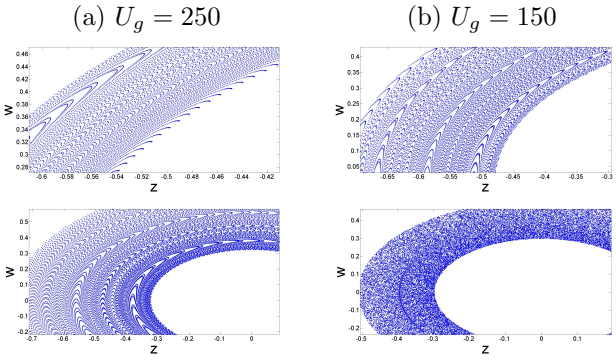

Figure 2: Poincaré maps for various U_g – undamped case

Figure 2 shows the Poincaré map of the undamped slow flow system. The map shown is magnified to show the formation of nonlinear resonance islands at $U_g = 250$. The resonance islands can be observed as elliptic formations, and the appearance of 'straight lines' in between the islands, known as invariant tori. Figures 2 also shows the Poincaré maps at $U_g = 150$ and $Ug = 100$. We can see that with the decrease in the value of the parameter U_g, the islands are slowly destroyed, implying that nonlinear resonances overlap to break the tori and produce chaotic motion as shown in figure 2(d) with the map filled with chaotic trajectories as shown.

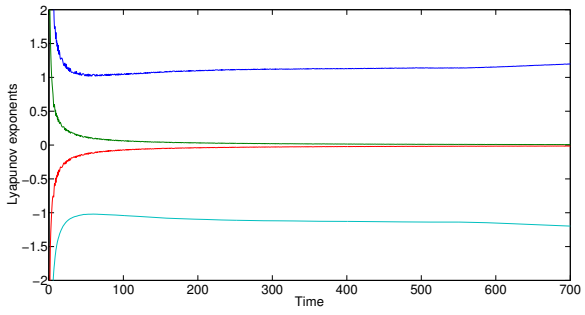

Figure 3: Plot of Lyapunov exponents at $U_g = 50$ – undamped case

To confirm chaos, we compute the largest Lyapunov exponent. In figure 3, the spectrum of Lyapunov exponents is shown for $U_g = 50$. It can be easily observed from this figure, that the largest Lyapunov exponent is positive, and hence chaos exists at $U_g = 50$.

Figures 4 and 5 show the numerical simulation of equation (19), representing the damped slow flow equations. The map shown in figure 4 (b) is magnified and one can

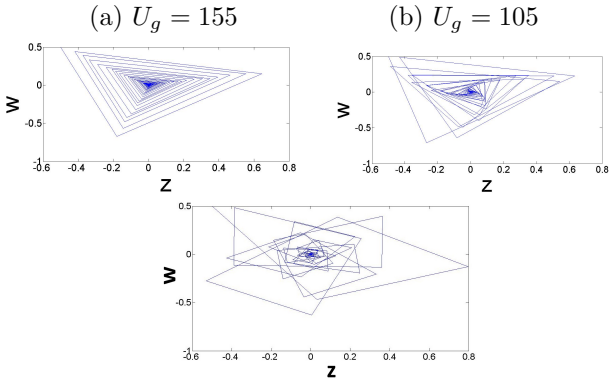

Figure 4: Phase plots for various U_g – damped case

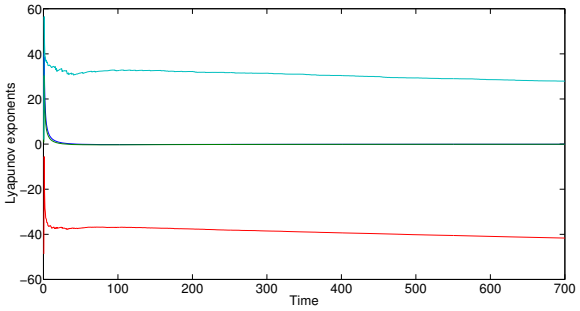

Figure 5: Spectra of Lyapunov exponents at $U_g = 105$ – damped case

observe the dissipative motion of the system towards the attractor and with the curves winding up on a attractor. In figure 5, the spectrum of Lyapunov exponents is shown for $U_g = 105$. It can be observed from this figure, that the largest Lyapunov exponent is positive, and hence chaos exists at $U_g = 105$ and the attractors shown in the phase plots for $U_g \leq 105$ are chaotic attractors.

From the numerical simulation results, it can be seen that the chaotic motion for the undamped slow flow equations appears at $U_g = 50$ and for the damped slow flow equations at $U_g = 105$. From extensive simulations, it was observed that for U_g greater than 150, there is no chaos for the undamped slow flow equations. If we assume that the rotating wind turbine blade has a uniform circular cross-section, using the parameter values in Table 1 and from equation (7) we obtain that an U_g value of 150 corresponds to $R \approx 34.08$ cm. Hence, to avoid chaotic motion, the radius of the blade must be more than 34.08 cm. Likewise, for the damped slow flow equations, for an U_g value greater than 200, no chaos is observed in

simulations. Using equation (7), the corresponding radius of the blade is $R \approx 45.44$ cm and hence, in order to avoid chaotic motion, the radius of the blade must be more than 45.44 cm. It may be noted that a rotating wind turbine blade will be subjected to torsion as well as bending and in that sense, the U_g and corresponding R values are only indicative. Nevertheless, the nonlinear dynamic analysis presented in this work can be used in design of wind turbine blades.

5 Conclusion

This paper deals with the nonlinear dynamics of a flexible rotating beam with large deformation and geometric nonlinearities. The equations of motion were obtained as a set of four ordinary differential equations and were non-dimensionalized using two characteristic velocities representing the speed of sound (U_a) and speed of transverse vibrations (U_g). A perturbation analysis was done to study the nonlinear system at a slower time scale and the slow flow equations were derived from the original nonlinear ordinary differential equations by the method of multiple scales. Both the undamped and damped system of equations were obtained and analyzed. The slow flow equations were simulated numerically to investigate the existence of chaos. From the numerical simulation results, it can be concluded that in both undamped and damped cases chaos is obtained below certain values of U_g. The practical application of this analysis would be in the design of a rotating wind turbine blades where the radius of the blade could be chosen to avoid chaotic motion.

References

[1] Hilborn R. C., Chaos and Nonlinear Dynamics: An Introduction to Scientists and Engineers, *Oxford University Press*, 2000.

[2] Nikolai A. M. and Sidorov S. V., New Methods for Chaotic Dynamics, *World Scientific Series on Nonlinear Science: Series A*, 2006.

[3] Nayfeh A. H. and Balachandran B., Applied Nonlinear Dynamics: Analytical, Computational and Experimental Methods, *Wiley-VCH Verlag GmbH and Co. KGaA*, 2004.

[4] Strogatz S. H., Nonlinear dynamics and chaos: With applications to Physics, Biology, Chemistry and Engineering, *Westview Press*, 2007.

[5] Sun J. Q. and Luo A. C. J., Bifurcations and Chaos in Complex Systems, *Edited Series on Advances in Nonlinear Science and Complexity*, Vol 1, 2006.

[6] Guckenheimer J. and Holmes P., Nonlinear Oscillations, Dynamical Systems, and Bifurcations of Vector Fields, *Applied Mathematical Sciences, Springer-Verlag, New York*, Vol 42, 1983.

[7] Thompson J. M. T. and Stewart H. B., Nonlinear Dynamics and Chaos, *2nd ed., John Wiley & Sons, Chichester*, 2002.

[8] Kovacic I. and Brennan M. J., The Duffing Equation: Nonlinear Oscillators and Their Behaviour, *1st ed., John Wiley & Sons, Ltd.*, 2011.

[9] Burov, A. A., On the non-existence of a supplementary integral in the problem of a heavy two-link plane pendulum, *J. of Applied Mathematics and Mechanics*, 50(1), 123-125, 1986.

[10] Lankalapalli S. and Ghosal A., Possible chaotic motion in a feedback controlled 2R robot, In *Proceedings of the 1996 IEEE International Conference on Robotics and Automation, Minneapolis, MN, April, N. Caplan and T. J. Tarn (eds.)*, pages 1241-1246. IEEE Press, New York, 1996.

[11] Nakamura Y., Suzuki T. and Koinuma M., Nonlinear behavior and control of a nonholonomic free-joint manipulator, *IEEE Transactions on Robotics and Automation*, 13(6), 853-862, 1997.

[12] Mahout V., Lopez P., Carcasss J. P. and Mira C., Complex behaviours of a two-revolute joints robot: Harmonic, subharmonic, higher harmonic, fractional harmonic, chaotic responses, In *Proceedings of the IEEE Systems, Man & Cybernetics '93 Conference, Le Touquet, France*, October 17-20, pp. 201-205, 1993.

[13] Verduzco F. and Alvarez J., Bifurcation analysis of a 2-DOF robot manipulator driven by constant torques, *International Journal of Bifurcation and Chaos*, 617-627, 1999.

[14] Li K. F., Li L. and Chen Y., Chaotic motion phenomenon in planar 2R robot, *Journal of Sichuan University of Science and Technology*, 21(l), 6-9, 2002.

[15] Yin Z. and Ge X., Chaotic Self-motion of a Spatial Redundant Robotic Manipulator, *Research Journal of Applied Sciences, Engineering and Technology*, 3(9), 993-999, 2011.

[16] Yang X. D. and Chen L. Q., Bifurcation and chaos of an axially accelerating viscoelastic beam, *Chaos, Solitons and Fractals*, 23, 249-258, 2005.

[17] Yu P., Bi Q., Analysis of nonlinear dynamics and bifurcations of a double pendulum, *Journal of Sound and Vibration*, 217(4), 691-736, 1988.

[18] Balachandran B. and Nayfeh A. H., Cyclic motions near a Hopf bifurcation of a four-dimensional system, *Nonlinear Dynamics*, 3(1), 19-39, 1992.

[19] Nayfeh A. H., Introduction to Perturbation Techniques, *John Wiley and Sons Inc.*, 1993.

[20] Wahi P. and Kumawat V., Nonlinear stability analysis of a reduced order model of nuclear reactors: A parametric study relevant to the advanced heavy water reactor, *Nuclear Engineering and Design*, 241, 134-143, 2011.

[21] Chandra Shaker M. and Ghosal, A., Nonlinear modeling of flexible link manipulators using non-dimensional variables, *Trans. ASME, Journal of Computational and Nonlinear Dynamics*, 1(2), 123-134, 2006.

[22] Endurance Wind Power Ltd., http://www.endurancewindpower.com/e3120.html (last accessed June 6, 2014)

[23] Nandakumar K., A study of four problems in nonlinear vibrations via the method of multiple scales, *Doctor of Philosophy Thesis*, IISc Bangalore, 2009 (available at http://hdl.handle.net/2005/950).

[24] El-Bassiouny A. F., Response of a three-degree-of-freedom system with cubic nonlinearities to harmonic excitation, *Applied Mathematics and Computation*, 104, 65-84, 1999.

[25] Cao D. X. and Zhang W., Global bifurcations and chaotic dynamics for a string-beam coupled system, *Chaos, Solitons and Fractals*, 2006.

[26] Jinchen J. and Yushu C., Bifurcation in a parametrically excited two degree of freedom nonlinear oscillating system with 1:2 internal resonance, *Applied Mathematics and Mechanics*, 20(4), 350-359, 1999.

[27] Parker T. S. and Chua L. O., Practical numerical algorithms for chaotic systems, *Springer Verlag New York Inc.*, 1989.

[28] Sandri M., Numerical Calculation of Lyapunov Exponents, *The Mathematica Journal*, 6(3), 78-84, 1996.

[29] Tsumoto K., Ueta T., Yoshinaga T. and Kawakami H., Bifurcation analyses of nonlinear dynamical systems: From theory to numerical computations, *Nonlinear theory and its applications IEICE*, 3(4), 458-476, 2012.

[30] MATLAB, *Version 8.0 (R2012b)*, The MathWorks Inc., Natick, Massachusetts, 2012.

[31] Michael B. Monagan, Keith O. Geddes, K. Michael Heal, George Labahn, Stefan M. Vorkoetter, James McCarron, and Paul DeMarco., *Maple 14 Programming Guide*, Maplesoft, Waterloo ON, Canada, 2012.

APPENDIX 1

The description of the terms given in equation (8) is presented in this section. It may be noted that all terms have been computed symbolically using Maple [31].

Symmetric mass matrix

$$\mathcal{M}(1,1) = \frac{1}{3} + \frac{2}{3}U_2 + \frac{1}{3}U_2^2 + \frac{13}{35}V_2^2 - \frac{11}{105}V_2\phi_2 + \frac{1}{105}\phi_2^2$$
$$\mathcal{M}(1,2) = -\frac{7}{20}V_2 + \frac{1}{20}\phi_2$$
$$\mathcal{M}(1,3) = \frac{7}{20} + \frac{7}{20}U_2,\ \mathcal{M}(1,4) = -\frac{1}{20} - \frac{1}{20}U_2$$
$$\mathcal{M}(2,2) = \frac{1}{3},\quad \mathcal{M}(2,3) = \mathcal{M}(2,4) = 0$$
$$\mathcal{M}(3,3) = \frac{13}{35},\quad \mathcal{M}(3,4) = -\frac{11}{210},\quad \mathcal{M}(4,4) = \frac{1}{105}$$

Conventional stiffness matrix

The non-zero elements of the symmetric stiffness matrix are

$$\mathcal{K}(3,3) = 4,\ \mathcal{K}(3,4) = -6,\ \mathcal{K}(4,4) = 4$$

Geometric stiffness matrix

The non-zero elements of the symmetric geometric stiffness matrix are

$$\Delta\mathcal{K}(2,2) = \frac{U_a^2}{U_g^2},\ \Delta\mathcal{K}(2,3) = \frac{U_a^2}{U_g^2}\left(\frac{3}{5}V_2 - \frac{1}{20}\phi_2\right)$$
$$\Delta\mathcal{K}(2,4) = \frac{U_a^2}{U_g^2}\left(-\frac{1}{20}V_2 + \frac{1}{25}\phi_2\right),\ \Delta\mathcal{K}(3,3) = \frac{U_a^2}{U_g^2}\left(\frac{3}{5}U_2\right)$$
$$\Delta\mathcal{K}(3,4) = -\frac{U_a^2}{U_g^2}\left(\frac{1}{20}U_2\right),\ \Delta\mathcal{K}(4,4) = \frac{U_a^2}{U_g^2}\left(\frac{1}{15}U_2\right)$$

Coriolis and centripetal terms

$$\begin{aligned}\mathcal{H}(1,1) &= \frac{2}{3}\dot{U}_2\dot{\theta}_1 + \frac{2}{3}U_2\dot{U}_2\dot{\theta}_1 + \frac{26}{35}V_2\dot{V}_2\dot{\theta}_1 \\ &\quad - \frac{11}{105}\phi_2\dot{V}_2\dot{\theta}_1 - \frac{11}{105}V_2\dot{\theta}_1\dot{\phi}_2 + \frac{2}{105}\phi_2\dot{\theta}_1\dot{\phi}_2 \\ \mathcal{H}(1,2) &= -\frac{7}{10}\dot{V}_2\dot{\theta}_1 - \frac{1}{3}\dot{\theta_1}^2 - \frac{1}{3}U_2\dot{\theta_1}^2 \\ \mathcal{H}(1,3) &= \frac{7}{10}\dot{U}_2\dot{\theta}_1 - \frac{13}{35}V_2\dot{\theta_1}^2 + \frac{11}{210}\phi_2\dot{\theta_1}^2 \\ \mathcal{H}(1,4) &= -\frac{1}{10}\dot{U}_2\dot{\theta}_1 + \frac{11}{210}V_2\dot{\theta_1}^2 - \frac{1}{105}\phi_2\dot{\theta_1}^2\end{aligned}$$

APPENDIX 2

Derivation of equations (11)

In section 3, we performed a multiple scales analysis of the rotating link. At order ϵ, four equations, given by equations (11) were obtained. The solution to those equations was given by equation (12). This section presents the derivation of this set of equations.
From equation (11), we get a system of coupled differential equations with constant coefficients whose solutions can be obtained by letting

$$\theta_{10} = c_1 e^{i\omega T_0}, U_{20} = c_2 e^{i\omega T_0}, V_{20} = c_3 e^{i\omega T_0}, \phi_{20} = c_4 e^{i\omega T_0} \tag{B-1}$$

Substituting (B-1) into (11), we get

$$\begin{aligned}&-\frac{1}{3}\omega^2 c_1 - \frac{7}{20}\omega^2 c_3 + \frac{1}{20}\omega^2 c_4 = 0 \\ &\left(\frac{U_a^2}{U_g^2} - \frac{\omega^2}{3}\right)c_2 = 0 \\ &-\frac{7}{20}\omega^2 c_1 + \left(12 - \frac{13}{35}\omega^2\right)c_3 + \left(\frac{11}{210}\omega^2 - 6\right)c_4 = 0 \\ &\frac{1}{20}\omega^2 c_1 + \left(\frac{11}{210}\omega^2 - 6\right)c_3 + \left(4 - \frac{1}{105}\omega^2\right)c_4 = 0\end{aligned} \tag{B-2}$$

For a non-trivial solution, the determinant matrix must be zero, i.e.,

$$\begin{vmatrix} -\frac{1}{3}\omega^2 & 0 & -\frac{7}{20}\omega^2 & \frac{1}{20}\omega^2 \\ 0 & \frac{U_a^2}{U_g^2} - \frac{\omega^2}{3} & 0 & 0 \\ -\frac{7}{20}\omega^2 & 0 & \left(12 - \frac{13}{35}\omega^2\right) & \left(\frac{11}{210}\omega^2 - 6\right) \\ \frac{1}{20}\omega^2 & 0 & \left(\frac{11}{210}\omega^2 - 6\right) & \left(4 - \frac{1}{105}\omega^2\right) \end{vmatrix} = 0 \tag{B-3}$$

The values of ω thus calculated are,

$$\omega_1 = 0, \omega_2 = \frac{\sqrt{3}U_a}{U_g}, \omega_3 = 70.0871, \omega_4 = 17.5444 \tag{B-4}$$

Substituting the values of ω in equation (11), we have

$$\text{When } \omega = \omega_1,\ c_{11} = c_{21} = c_{31} = c_{41} = 0 \tag{B-5}$$
$$\text{When } \omega = \omega_2,\ c_{12} = c_{32} = c_{42} = 0, c_{22} = 1 \tag{B-6}$$
$$\text{When } \omega = \omega_3,\ c_{13} = 1, c_{23} = 0, c_{33} = -0.8222, \quad c_{34} = 0.9112 \tag{B-7}$$
$$\text{When } \omega = \omega_4,\ c_{41} = 1, c_{42} = 0, c_{43} = -1.2789, \quad c_{44} = -2.2856 \tag{B-8}$$

The general solution of equation (11) can be written as,

$$\begin{aligned}\begin{bmatrix}\theta_{10}\\U_{20}\\V_{20}\\\phi_{20}\end{bmatrix} &= A_1 e^{i\omega_1 T_0}\begin{bmatrix}c_{11}\\c_{21}\\c_{31}\\c_{41}\end{bmatrix} + A_2 e^{i\omega_2 T_0}\begin{bmatrix}c_{12}\\c_{22}\\c_{32}\\c_{42}\end{bmatrix} \\ &\quad + A_3 e^{i\omega_3 T_0}\begin{bmatrix}c_{13}\\c_{23}\\c_{33}\\c_{43}\end{bmatrix} + A_4 e^{i\omega_4 T_0}\begin{bmatrix}c_{14}\\c_{24}\\c_{34}\\c_{44}\end{bmatrix}\end{aligned} \tag{B-9}$$

which is identical to the form in equation (12).

Terms in equation (16-17)

$$\begin{aligned}J_{22} &= \frac{1}{20}(c_{43} - 7c_{33})\omega_3^2 - \frac{U_a^2}{U_g^2}\left(\frac{3}{5}c_{33}^2 + \frac{c_{43}^2}{15} - \frac{c_{33}c_{43}}{10}\right) \\ &\quad - \frac{7}{10}c_{33}\omega_3^2 - \frac{\omega_3^2}{3}, Z_{11} = -\frac{2}{3} - \frac{7c_{33}}{10} + \frac{c_{43}}{10}\end{aligned}$$

$$Z_{12} = (\omega_3 - \omega_2)\left(\frac{2}{3}\omega_3 + (\omega_3 + \omega_2)\left(\frac{7c_{33} - c_{43}}{20}\right)\right)$$
$$Z_{31} = -\frac{7}{10} - \frac{26c_{33}}{35} + \frac{11c_{43}}{105}$$

$$Z_{32} = \frac{7\omega_3}{20}(\omega_3 - 2\omega_2) + \frac{U_a^2}{U_g^2}\left(-\frac{6c_{33}}{5} + \frac{c_{43}}{10}\right)$$

$$Z_{41} = \frac{1}{10} + \frac{11c_{33}}{105} - \frac{2c_{43}}{105}, \quad Z_{w1} = \frac{\omega_3^4}{3780} - \frac{34\omega_3^2}{105} + 4$$

$$Z_{42} = \frac{\omega_3}{20}(2\omega_2 - \omega_3) + \frac{U_a^2}{U_g^2}\left(\frac{c_{33}}{10} - \frac{2c_{43}}{15}\right)$$

$$Z_{w3} = \frac{11\omega_3^2}{30} - \frac{\omega_3^4}{4200}, \quad Z_{w4} = \frac{\omega_3^2}{2} + \frac{\omega_3^4}{12600}$$

$$Z_{d1} = \alpha\left(-\frac{1}{3} - \frac{7c_{33}}{20} + \frac{c_{43}}{20}\right)$$

$$Z_{d3} = \left(-\frac{7\alpha}{20} - \left(\frac{13\alpha}{35} + 12\beta\right)c_{33} + \left(\frac{11\alpha}{210} + 6\beta\right)c_{43}\right)$$

$$Z_{d4} = \left(\frac{\alpha}{20} + \left(\frac{11\alpha}{210} + 6\beta\right)c_{33} - \left(\frac{\alpha}{105} + 4\beta\right)c_{43}\right)$$

where c_{33}, c_{43} were calculated in the preceding section of this appendix.